Analyzing Dynamic P-Q Capability and Operational Abnormalities of PMSG Wind Turbines

Shahinur Rahman, Shuhui Li, Himadry Shekhar Das
Electrical and Computer Engineering Department
The University of Alabama, Tuscaloosa
Email: srahman6@crimson.ua.edu, sli@eng.ua.edu, hdas@crimson.ua.edu

Abstract—With the proliferation of large-scale grid-connected wind farms, subsynchronous oscillations (SSOs) incidents associated with Type-4 wind turbines (WTs) with a permanent magnet synchronous generator (PMSG) occurred frequently. These incidents have caused severe reliability risks to the power grid. Conventionally, P-Q capability charts are utilized to ensure the safety operating region of a synchronous generator. However, a PMSG WT exhibits a complete different and dynamic P-Q capability characteristics due to the difference in energy conversion technique and several other critical factors related to the power converters of the WT. This paper presents a comprehensive dynamic P-Q capability study of a PMSG WT with sufficient and accurate considerations of the WT control and operation in the dq reference frame, its specific power converter constraints, variable grid conditions, etc. Models of a PMSG WT are first developed based on its control principle in the dq reference frame. Then, algorithms for obtaining the P-Q capability charts of the WT are developed with the considerations of complete WT constraints in different aspects. The proposed study is verified via an electromagnetic transient (EMT) model of a grid-connected Type-4 WT.

Index Terms—Permanent magnet synchronous generator (PMSG), P-Q capability charts, subsynchronous oscillation (SSO), d-q vector control.

I. Introduction

Wind power has been becoming a primary renewable energy source in the electric power systems to replace power generated from conventional synchronous generators (SGs). Traditionally, for safe operation of a SG, the control capability of the generator is defined by "Capability Charts" or "Operating Charts" [1]. In the same way, the power industry has specified P-O capability charts for Type-4 WTs to ensure a stable and reliable operation of the WTs [2], [3]. However, a PMSG WT is totally different from a traditional SG. Instead of operating at a fixed speed and be connected to the grid directly, a PMSG WT operates in a wide speed range from 0 rpm to over the synchronous speed of the WT generator and is connected to the grid via a full-scale back-to-back ac/dc/ac voltage-source converter (VSC) [4], all of which would affect the operating characteristics of the WT. Thus, the PQ capability charts of a PMSG WT would be highly dynamic and completely distinct from those of a traditional SG.

So far, no attempt has been taken to investigate the dynamic P-Q capability of a PMSG WT considering these factors. In [5], the reactive power capability of PMSG WTs is discussed in terms of modulation technique and rated current boundary of power converters, however, generator characteristics and PWM voltage saturation limit of power converters

are not addressed. The authors proposed a distributed demand response control of PMSG-based WTs in [6], which incorporates the reactive power sharing capability based on fixed P-Q capability charts. Therefore, the proposed framework of [6] only operates well in a nominal voltage condition. To operate PMSG-based WTs robustly in different grid situations, several control strategies are described in [7], [8], which consider MPPT capability along with generator speed variations but ignore the P-Q capability of power converters. In [9], the authors proposed an approach to improve the operation and performance of Type-4 wind power plants by adding a synchronous condenser. However, adding extra reactive power from an outside source can only mitigate certain burdens for the PMSG WTs. In the long run, this strategy will fail to maintain the WT operation within its safety boundary under uncertain and variable real-life grid conditions.

Therefore, it is important to conduct a detailed study on PMSG P-Q capability characteristics. Without such a study, one would be misled by many abnormal PMSG WT operation phenomena and unable to develop advanced PMSG control technology to overcome the challenges. A study on the P-Q capability characteristics of a Type-3 WT is conducted in [10]. However, a Type-4 WT has a structure that is completely different from that of a Type-3 WT. As a result, a detailed dynamic P-Q capability study of Type-4 PMSG WTs is presented in this paper by considering the MPPT capability of the WT generator, power converter constraints (such as PWM saturation limit and rated current boundary), and variable and uncertain operating conditions of the power grids. The main contributions of the paper include: (1) Active and reactive power models of the combined PMSG WT generator and power converters are developed in the dq reference frame. (2) Algorithms are exploited to determine the dynamic P-Q capability charts of a PMSG WT by considering the different WT generator and power electronic converter constraints. (3) Dynamic P-Q capability charts of the PMSG WT are studied under variable WT speed and grid conditions. (4) Integrated P-Q capability characteristics of the overall PMSG WT are investigated. (5) Several case studies through EMT simulation are conducted to reveal the root cause of abnormal operations associated with PMSG WTs and the significance of dynamic P-Q capability charts to understand irregular operations of Type-4 WTs and wind plants reported in the literature.

The remainder of this paper is organized in the following way. Section II explains briefly the key features of a PMSG WT and its MPPT control technique. The active and reactive

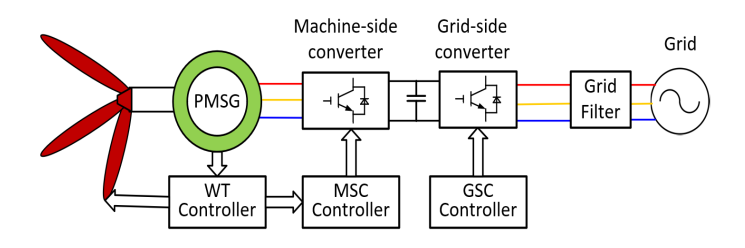


Fig. 1: A PMSG wind turbine system.

power models of the PMSG WTs is developed in the dq reference frame in Section III. Section IV describes the algorithms to determine PMSG WT P-Q capability charts. Section V evaluates the PMSG dynamic P-Q capability characteristics. Section VI shows several simulated case scenarios of PMSG WT abnormal operation and section VIII provides the concluding remarks.

II. PMSG WT AND ITS CONTROL

A PMSG WT is made of three components: (i) a wind turbine, (ii) a PMSG, and (iii) two VSCs connected in a row (Fig. 1). In the turbine, the blades extract wind power and transfer it to the PMSG. The PMSG converts wind energy (mechanical) into electrical energy.

A. MPPT control

The mechanical power extracted by a WT from the wind is written by a popular cube law equation as in (1).

$$P_{w} = \frac{1}{2} \rho_{air} A_{blade} C_{P}(\beta, \lambda) v_{w}^{3}$$

$$\lambda = R_{blade} \omega_{m} / v_{w}$$
(1)

where v_w , R_{blade} , ω_m , and A_{blade} represent the wind velocity in m/s, WT blades' radius in meters, WT blades' rotational speed in rad/s, and rotor blade swept area in m^2 accordingly. ρ_{air} defines the air density in kg/m^3 . C_P is a constant to measure the performance efficiency of a WT. It is calculated from tip-speed-ratio (λ) and pitch angle (β) of rotor blades using aerodynamic laws, therefore, may differ from one WT to another. The mathematical expression of C_P is found from a curve fitting equation as in (2), where the value of a_{ij} coefficients is obtained in [11]. For each β , there exists an optimum tip-speed-ratio (λ_{opt}) for which C_P will get the largest value (i.e., extract maximum energy for that β). At a normal wind velocity, the rotor blades' angular speed is managed to an optimal magnitude ($\omega_{m_{opt}}$) via PMSG controls so that $\lambda_{opt} = R_{blade} \omega_{m_opt} / v_w$ while keeping β unchanged. At a high wind speed, the captured wind power exceeds the rated power of the machine. In that situation, a control signal is energized to limit the power generation beyond the rated value by regulating β .

$$C_P(\beta, \lambda) = \sum_{i=0}^4 \sum_{j=0}^4 a_{ij} \beta^i \lambda^j$$
 (2)

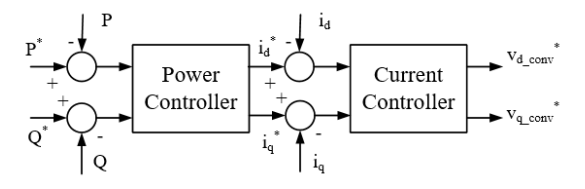


Fig. 2: Concept of MSC and GSC controllers of the PMSG WTs.

B. PMSG WT control

Typically, a PMSG WT has three control blocks: (i) a WT control block, (ii) a MSC control block, and (iii) a GSC control block (Fig. 1). The WT control block generates a power/speed reference signal using maximum power extraction principle. Following the speed/power reference, the MSC control block regulates the angular speed of PMSG and fulfills the maximum wind energy extraction goal. The GSC control block keeps the dc-link voltage constant and controls the reactive power generation/absorption of the PMSG. Typically, rotor-flux orientation frame is used to design the MSC control block and the PCC voltage orientation frame is used to design the GSC control block. Both MSC and GSC control blocks can be considered to have two loops (Fig. 2): (i) an inner current control loop and (ii) an outer active and/or reactive power control loop. Usually, the control loops are modeled in the dq reference frame. The power and current control loops generate d- and q-axis reference currents $(i_d^* \text{ and } i_q^*)$ and voltages $(v_{d\ conv}^* \text{ and }$ $v_{q_conv}^*$), respectively. According to the average model of a converter, the voltage (v_{dq_conv}) injected to the MSC/GSC ac side is expressed as in (3).

$$v_{dq_conv} = k_{PWM}.v_{dq_conv}^* \tag{3}$$

where k_{PWM} is the ratio of the voltage at the MSC/GSC ac side to the PWM controlled voltage of the MSC/GSC.

III. P-Q MODEL OF A PMSG WT

To find a dynamic P-Q capability chart, the P-Q model of PMSG WTs must be developed including the MSC and GSC control in the dq reference frame. Therefore, in this paper, P-Q capability analysis of the PMSG WTs includes: (i) MSC P-Q model, (ii) GSC P-Q model, and (iii) combined MSC and GSC P-Q model.

A. MSC P-Q model

Using the generator sign, PMSG stator voltage, and flux linkage in the dq reference frame are obtained in the following way:

$$v_{s_dq} = -R_s i_{s_dq} - \frac{d}{dt} \psi_{s_dq} + j\omega_e \psi_{s_dq}$$
 (4)

$$\psi_{s_dq} = (L_{ls} + L_m)i_{s_dq} + \psi_f \tag{5}$$

where R_s and L_{ls} are resistance and leakage inductance of the stator winding, L_m is the mutual inductance, ω_e is the electrical angular velocity of the PMSG, and ψ_f is the flux linkage generated by the permanent magnet (PM).

In (4), the stator dq voltage (v_{s_dq}) is defined as $v_{s_dq} = v_{sd} + jv_{sq}$, where v_{sd} and v_{sq} are d- and q-axis components. In the same way, stator dq current (i_{s_dq}) and stator dq flux (ψ_{s_dq}) are defined.

For a steady-state condition, (6) is obtained from (4) and (5), in which I_{s_dq} and V_{s_dq} define the steady-state dq stator current and voltage, respectively.

$$V_{s\ dq} = -R_s I_{s\ dq} - j\omega_e (L_{Ls} + L_m) I_{s\ dq} + j\omega_e \psi_f \qquad (6)$$

The active (P_s) and reactive (Q_s) power passing through the MSC to the dc-link can be written as in (7). Note that P_s is positive, i.e., generating power from the stator path to the MSC.

$$P_s + jQ_s = V_{s_dq} I_{s_dq}^* \tag{7}$$

B. GSC P-Q model

Typically, the PMSG GSC is tied to the power grid through a LCL, LC, or L filter. The development of the GSC P-Q model having any of these three filtering configurations is the same. In this study, a GSC connected to the grid via an L filter will be focused. In the L filtering scheme, L_f and R_f define the filter inductance and resistance, accordingly. Considering the generation sign principle, the voltage balance equation in the dq reference frame is expressed as in (8).

$$v_{GSC_dq} = R_f i_{dq} + L_f \frac{d}{dt} i_{dq} + j\omega_s L_f i_{dq} + v_{dq}$$
 (8)

where ω_s is the grid angular frequency. v_{dq} , and v_{GSC_dq} denote the d- and q-axis of PCC voltage and GSC output voltage, accordingly. i_{dq} represents the d- and q-axis current components flowing through the GSC to the ac power grid.

For the steady-state condition, (8) can be written as (9), where I_{dq} , V_{dq} , and V_{GSC_dq} define the steady-state dq components of the L-filter current, grid voltage, and GSC output voltage.

$$V_{GSC\ dq} = R_f I_{dq} + j\omega_s L_f I_{dq} + V_{dq} \tag{9}$$

Following the PCC voltage orientation, the active and reactive power coming from the GSC and injecting to the ac power grid is expressed as in (10).

$$P_{GSC} + jQ_{GSC} = V_{dq}I_{dq}^* = V_dI_d - jV_dI_q$$
 (10)

C. Combined MSC and GSC P-Q model

The active power transferred to the MSC will be eventually fed to the power grid via the GSC. However, the reactive power transferred to the grid includes just the GSC reactive power. Therefore, the aggregated P-Q model of MSC and GSC can be written as follows.

$$P_{PMSG} = P_{GSC} = P_s$$

$$Q_{PMSG} = Q_{GSC}$$
(11)

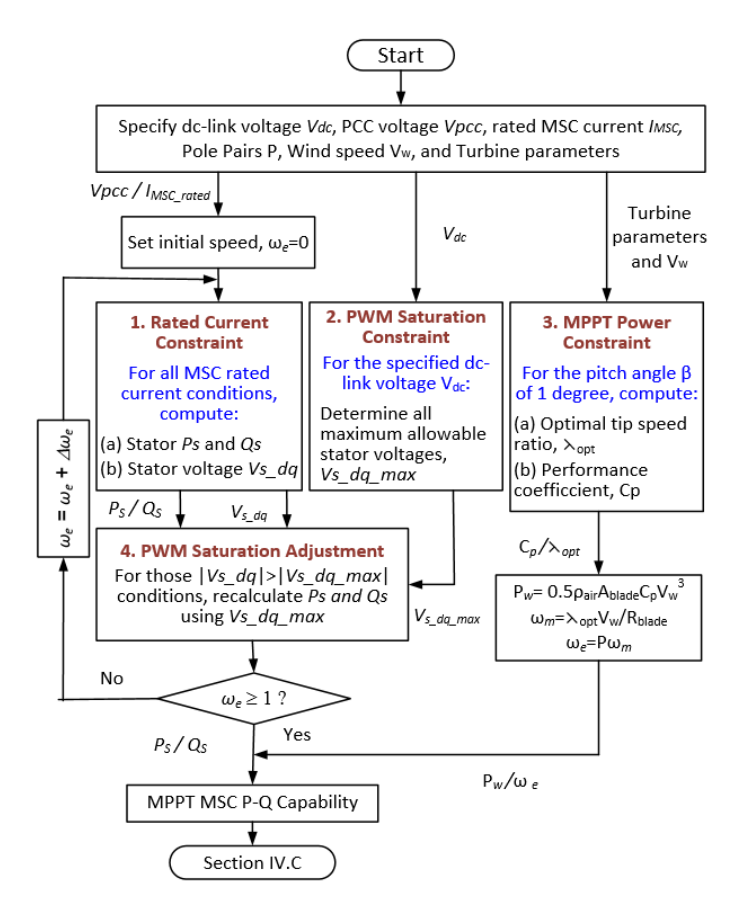


Fig. 3: A flowchart to find the PMSG P-Q capabilities considering the MSC PWM saturation and rated current limits.

IV. DETERMINE PMSG PQ CAPABILITY CHARTS

Primarily, a PMSG WT operation depends on the following limiting factors: (i) MSC current/power ratings, (ii) MSC PWM saturation constraint, (iii) GSC current/power ratings, and (iv) GSC PWM saturation boundary. To obtain PMSG P-Q capability charts, the above limiting factors should be kept in proper consideration.

A. Determine the MSC P-Q capability chart

Let us consider that S_{s_rated} is the rated apparent power of the PMSG stator. Therefore, the reference P_{MSC}^* and Q_{MSC}^* commands sent to the MSC control block should follow the below equation:

$$\sqrt{(P_{MSC}^*)^2 + (Q_{MSC}^*)^2} \le S_{s_rated}$$
 (12)

where P_{MSC}^* is positive (i.e., generating). Q_{MSC}^* would be either positive or negative.

However, (12) is not appropriate when the system does not operate at the nominal condition. For example, in a real-life situation, the dc-link voltage may drop significantly when the wind speed declines sharply. In that case, the MSC P-Q capability found by (12) would cause a higher current compared to the nominal current ratings. As MSC is very

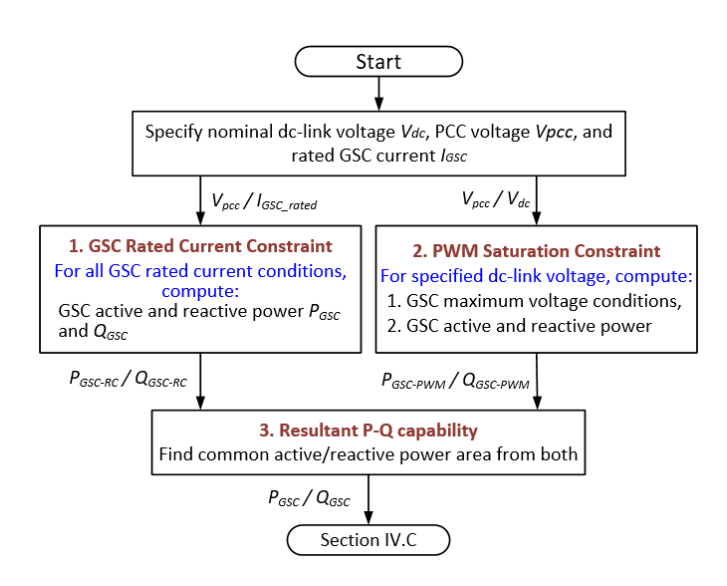


Fig. 4: A flowchart to find PMSG P-Q capabilities considering the GSC PWM saturation and rated current limits.

sensitive to current, it is important to use (13) instead of (12) to obtain the MSC P-Q capability charts.

$$\sqrt{(I_{d_MSC}^*)^2 + (I_{q_MSC}^*)^2} \le I_{MSC_rated}$$

$$\sqrt{(I_{sd}^*)^2 + (I_{sq}^*)^2} \le I_{sdq_rated}$$
(13)

Considering PWM saturation boundary, the d- and q-axis control voltages of MSC fed to the PMSG stator circuit would follow the equation below:

$$\sqrt{(v_{d_MSC})^2 + (v_{q_MSC})^2} \le V_{dq_MSC_max}$$

$$\sqrt{(v_{sd}^*)^2 + (v_{sq}^*)^2} \le V_{sdq_max}$$
(14)

where $V_{dq_MSC_max}$ is calculated by $V_{dc}/\sqrt{2}$ for space vector PWM (SVPWM) method. For sinusoidal PWM (SPWM) technique, $V_{dq_MSC_max}$ can be expressed by $\sqrt{3}V_{dc}/(2\sqrt{2})$.

Therefore, a flow chart to find the MSC P-Q capability together with the WT MPPT characteristics for wind power extraction is developed in Fig. 3 based on both rated current limit (13) and PWM saturation constraint (14). The flowchart has four major blocks. Block-1 computes the MSC P-Q capability based on the MSC current ratings only. For each condition, the stator voltage (V_{s_dq}) is kept in the record. Block-2 finds V_{s_dq} based on the PWM saturation boundary only. The WT MPPT power for pitch angle β of 1 degree is calculated in Block-3. In Block-4, V_{s_dq} recorded in Block-1 is reevaluated according to (14) to obtain the allowable stator voltage area. Then, the MSC P-Q capability chart is redetermined. The variable speed of the PMSG is defined by ω_e in the flowchart.

B. Determine the GSC P-Q capability chart

Alike the MSC, PWM saturation and rated current limits should be considered to find the GSC P-Q capability charts.

The reference current signals sent to the GSC control block have to meet the below equation:

$$\sqrt{(I_{d_GSC}^*)^2 + (I_{q_GSC}^*)^2} \le I_{GSC_rated}$$
 (15)

Following the PWM saturation boundary, the d- and q-axis control voltages of the GSC fed to the power grid should satisfy the below equation:

$$\sqrt{V_{d_GSC}^2 + V_{q_GSC}^2} \le V_{dq_GSC_max} \tag{16}$$

where $V_{dq_GSC_max}$ is $\sqrt{3}V_{dc}/(2\sqrt{2})$ for SPWM and $V_{dc}/\sqrt{2}$ for SVPWM.

Considering both PWM saturation and rated current constraints, a flow chart is developed in Fig. 4 to find the GSC P-Q capability chart. The flowchart has three major blocks. The first two blocks (Block-1 and -2) compute the GSC P-Q capability based on the rated current and GSC PWM saturation limits separately. Block-3 calculates the final GSC P-Q capability from the common areas of the previous two blocks.

C. Determine PMSG WT P-Q capability chart

Neglecting the converter power loss, active power transferred to the ac power grid via the GSC equals the active power transferred through the stator, i.e., $P_{GSC} = P_s$. Besides, reactive power transferred to the grid depends only on the reactive power generated/absorbed by the GSC that can be found from Fig. 4. Thus, the active power capability of the PMSG WT is found from the MSC active power capability. On the other hand, the reactive power capability is determined via the GSC reactive power capability.

V. ANALYZING DYNAMIC P-Q CAPABILITY CHARTS

A PMSG WT is modeled with the specifications given in [12] to analyze the dynamic P-Q capability chart. In this paper, all P-Q capability charts are shown in per unit. PCC line voltage (690V rms) and nominal PMSG power (2.0 MVA) are considered as the base voltage and base power in the per unit calculation.

A. Analyzing P-Q capability for the nominal case

The PCC voltage is 1 p.u. for the nominal case. Considering 1400V as the dc-link voltage and SPWM as the converters' modulation technique, the maximum stator voltage $(V_{s_dq_max})$ would be $\sqrt{3}V_{dc}/(2\sqrt{2}V_{base})=1.2425$ p.u. The inductance and resistance of the filter are considered as 0.2mH and 0.003 Ω , respectively. According to the flowcharts described in Section IV, the P-Q capability charts of the MSC, GSC, and PMSG WT MPPT are calculated and shown in Fig. 5. To observe the speed variation effect in the PMSG operation, all P-Q capability charts are plotted in the three-dimensional planes. Fig. 5 shows that the MPPT curves are within the MSC rated current P-Q capability area. This indicates that the power extracted by the WT can be transferred fully through the MSC from the rated current perspective. At zero speed, the MSC P-Q capability region is shown by the

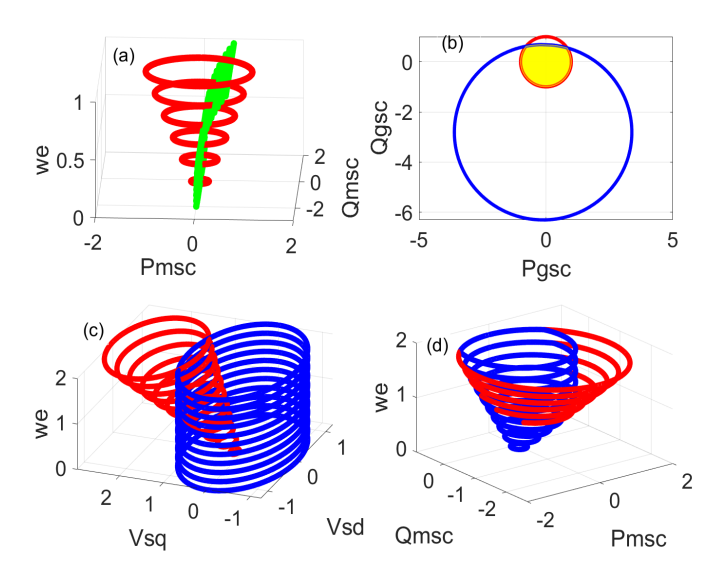


Fig. 5: PMSG P-Q capability curves at the nominal operating case: (a) MPPT curves (green) and MSC P-Q capability (red) for the MSC rated current constraint only, (b) GSC P-Q capability for the GSC PWM saturation (blue) and rated current (red) limits, (c) Stator voltage for the MSC rated current (red) and PWM saturation (blue) constraints, (d) MSC P-Q capability for the PWM saturation (blue) and rated current (red) limits.

smallest circle. Gradually the capability area increases with the higher speed (Fig. 5a). The GSC P-Q capability region (yellow) is encompassed by the area of the GSC capability considering both PWM saturation and rated current constraints (Fig. 5b). For a higher wind speed, a high stator voltage is required to convert wind energy until crossing the PWM saturation boundary (Fig. 5c). At a high wind speed, active power transfer through the MSC is limited for the PWM saturation boundary (Fig. 5d).

B. PQ capability at non-nominal and varying conditions

More studies were conducted to investigate the PQ capability characteristics under non-nominal and other varying conditions, such as different pole pairs, change in the dclink voltage, increase/decrease in PCC voltage, etc. The study found that high pole machines produce more flux compared to low pole machines that enlarge the MSC P-Q capability charts and allow to transfer of more extracted energy through the MSC. For the MSC, a smaller speed range is allowable for the high pole PMSG energy conversion until crossing the MSC PWM saturation boundary. The active power extracted from the high pole PMSG WT cannot be transferred fully through the MSC due to PWM saturation constraint.

Regarding the dc-link voltage, it was found that for the MSC, the larger the dc-link voltage is, the higher speed range would be allowable to convert wind energy until crossing the MSC PWM saturation boundary. For the same speed, the larger the dc-link voltage is, the more energy can be transferred through the MSC. For the GSC, a small voltage at the dc-link will shrink the P-Q capability region, whereas a larger dc-link voltage expands the area.

In terms of the PCC voltage, it was found that change in the PCC voltage cannot affect the MSC P-Q capability charts. For the GSC, a small PCC voltage shrinks P-Q capability curves under both PWM saturation and rated current constraints. On the other hand, a larger PCC voltage expands the curves. However, the curves move apart from one another. Therefore, the resultant GSC P-Q capability area decreases.

In summary, the PQ capability of a PMSG WT is highly dynamic and can be affected by varying grid and WT conditions.

VI. EMT SIMULATION MODEL FOR ANALYZING OPERATION OF PMSG WTS

To understand the significance of dynamic P-Q capability for secure and reliable power system operation, an EMT model with control of a grid-connected wind power plant containing Type-4 PMSG WTs is built using MATLAB/Simulink (Fig. 6). In the model, parameters specified in [12] are used for the PMSG WT and the plant model is an aggregated plant model with N Type-4 WTs. If N=1, the model reduces to a grid-connected Type-4 WT EMT model.

A. GSC Controller of a PMSG WT

Fig. 7 presents the existing GSC control method used in the PMSG industry. The standard vector control approach is used to control the GSC. The GSC controller has a nested-loop configuration. It consists of an inner current control loop and an outer control loop. The reference signal of the reactive power in the outer loop is limited by the nominal P-Q capability chart. For this purpose, a reactive power limitation block is modeled. The block calculates allowable reactive power generation/absorption limit (Q_{max}) and Q_{min} from the active power reference signal P_{PCC}^* shown in Fig. 8 and the P-Q capability area specified by the ERCOT or NERC.

Another block is modeled to limit the d- and q-axis reference currents coming from the outer control loop. If the condition $\sqrt{I_{d_GSC}^* + I_{q_GSC}^*}^2 \geq I_{dq_GSC_rated}$ satisfies, the block limits reference currents presented to the inner current controller following the Active Power Priority control mode as shown by

$$i_{d_GSC}^* \leftarrow i_{d_GSC}^*$$
 $i_{q_GSC}^* \leftarrow \text{sign}(i_{q_GSC}^*) \sqrt{(I_{dq_GSC_rated})^2 - (i_{d_GSC}^*)^2}$
(17)

To operate the GSC within the PWM saturation boundary, a block is modeled to adjust the voltages coming from the inner control loop as follows.

$$v_{d_GSC}^* \leftarrow V_{dq_GSC_max}.cos(\angle v_{dq_GSC}^*) v_{d_GSC}^* \leftarrow V_{dq_GSC_max}.sin(\angle v_{dq_GSC}^*)$$
(18)

B. MSC Controller of the PMSG WT

Fig. 8 presents the traditional MSC control method used in the PMSG industry. The standard vector control technique in

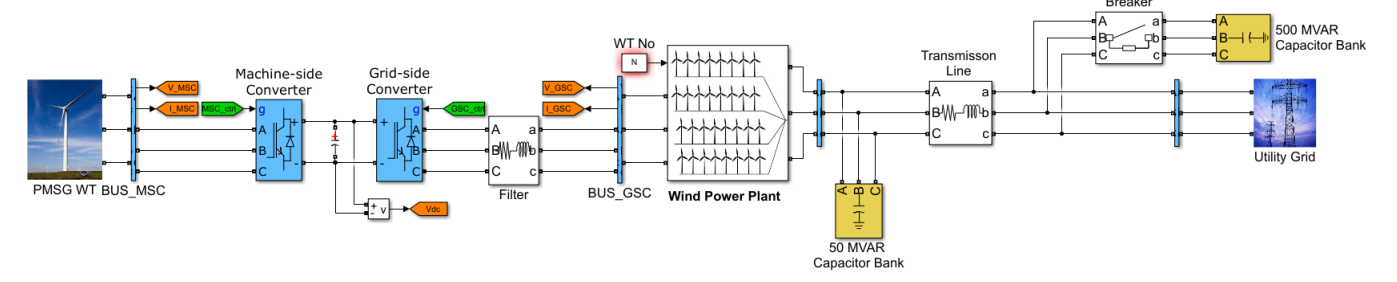


Fig. 6: EMT model and control of a PMSG WT built in MATLAB/Simulink software.

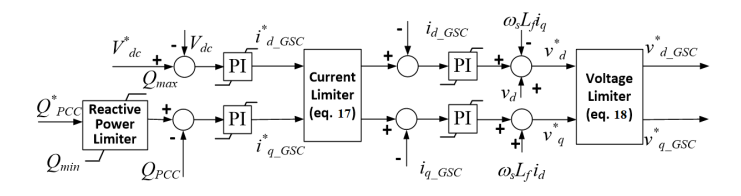


Fig. 7: Standard vector control diagram modeled in the GSC.

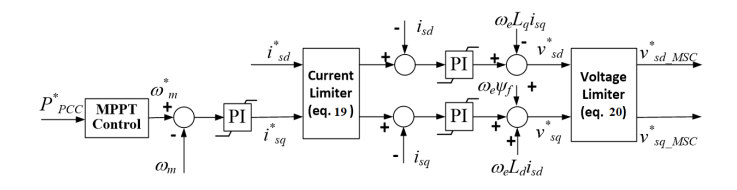


Fig. 8: Standard vector control diagram modeled in the MSC.

the rotor-flux orientation plane is built into the MSC controller. Alike GSC, it also has a faster inner current control loop and a slower outer power/speed control loop. A $P-\omega$ lookup table is modeled to extract maximum energy from the wind. The table generates a speed reference for the outer-loop speed controller. Based on the reference signal, the speed controller controls the generator angular speed and extract maximum wind energy.

A block is modeled to limit the d- and q-axis reference currents generated by the outer control loop based on the Active Power Priority Mode control, which is implemented in the current limitation block as follows.

$$i_{sd}^* \leftarrow \operatorname{sign}(i_{sd}^*) \sqrt{(I_{sdq_rated})^2 - (i_{sq}^*)^2}$$

$$i_{sq}^* \leftarrow i_{sq}^*$$

$$(19)$$

To operate the MSC within the PWM voltage saturation boundary, another block is modeled to control the voltages produced by the current control loop as follows.

$$v_{sd}^* \leftarrow V_{sdq_max}.cos(\angle v_{sdq}^*)$$

$$v_{sq}^* \leftarrow V_{sdq_max}.sin(\angle v_{sdq}^*)$$
(20)

VII. ANALYZING ABNORMAL OPERATION OF PMSG WTS

In this section, three case studies, including one industry case reported in the literature, are conducted to evaluate

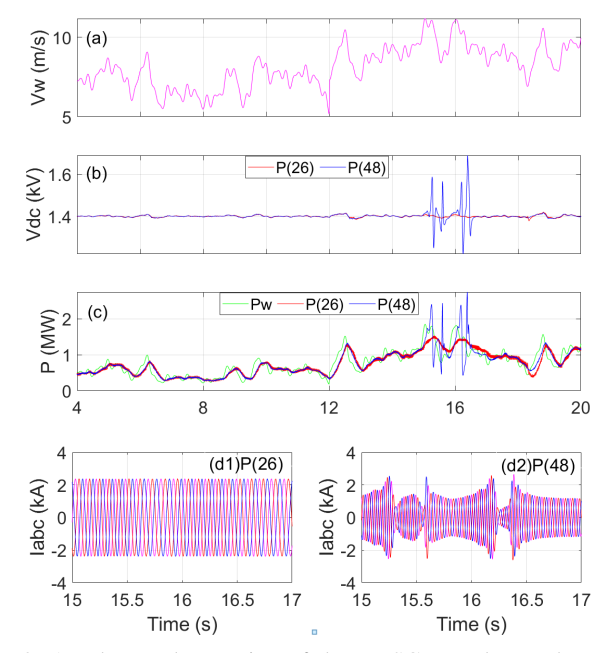


Fig. 9: An abnormal operation of the PMSG WT due to the MSC. a) wind speed variation, b) voltage at the dc-link, c) active power injected to the PCC, and d) Three-phase currents at the PCC.

the abnormal operations of PMSG WTs from dynamic P-Q capability perspectives.

A. Case Study 1: An abnormal operation due to the MSC

In this case, one 2 MVA PMSG WT is connected to the grid. A variable wind speed as shown in Fig. 9(a) is applied to the WT. Fig. 9 compares the control performance of the PMSG WT with two different pole numbers: (a) P = 26 and (b) P = 2648. The other WT parameters are kept the same as [12]. Fig. 9(c) shows the MPPT power during the simulation time frame. For the GSC, the reactive power reference is kept at 0 MVar. Therefore, the active and reactive powers generated by the WT follow both the ERCOT's and NREC's regulations. For the PMSG with 26 pole pairs, MSC can control the rotating speed of the WT and extract the maximum power from the wind (Fig. 9(c)) and GSC also maintains the dc-link voltage stability as shown in Fig. 9(b). However, active power and dc-link voltage fail to maintain stability at high wind speed for the PMSG WT with higher no of pole pairs (P = 48)and an abnormal phenomenon is observed, which may cause

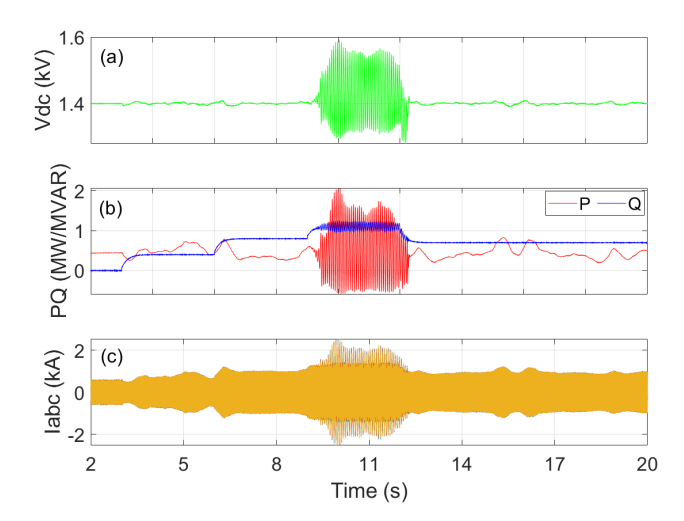


Fig. 10: An abnormal operation of the PMSG WT due to the GSC and its impact on: a) voltage at the dc-link, b) active and reactive power injected to the PCC, and c) Three-phase currents at the PCC.

severe damage to the WT. The results are consistent with the study shown in Section V-B. The case study reveals that the existing PMSG P-Q capability chart and control methods cannot address variable nature of PMSG WT P-Q capability and ensure safe and reliable power system operation.

B. Case Study 2: An abnormal operation due to the GSC

In this case, a situation was investigated when the actual dynamic P-Q capability of the GSC is not similar to ERCOT's or NERC's P-Q capability curve. To simulate the situation, NERC's P-Q capability chart is modeled in the GSC control block. The wind speed is the same as that of of Fig. 9(a). The reactive power reference is kept fixed at 0 MVar between 0-3 sec, 0.40 MVar between 3-6 sec, 0.80 MVar between 6-9 sec, 1.1 MVar between 9-12 sec, and 0.70 MVar after 12 sec. The references are set in such a way so that the active and reactive powers stay within the P-Q capability area defined in [2]. During the simulation, an abnormal operation event is observed for a higher reactive power demand (9-12 sec), which may damage the WT severely. The reason behind this occurrence is the use of a static P-Q capability chart (specified in [2]) instead of a dynamic one which encompasses the common area between the rated current and PWM saturation constraint circles (yellow area in Fig. 5b). On the other hand, P-Q capability chart in [2] considers the rated current boundary only (red circle in Fig. 5b). The abnormal operation occurs when the active and reactive power generated by the PMSG WT was outside the yellow area but within the red circle. Besides, the PCC voltage increases when the WT starts to generate power and inject into the grid. This increase in the PCC voltage causes the GSC P-Q capability chart to shrink.

C. Case Study 3: An abnormal operation due to the capacitor bank switching

This is a real industry case regarding an irregular operation of HydroOne's Type-4 wind farm that was caused by the

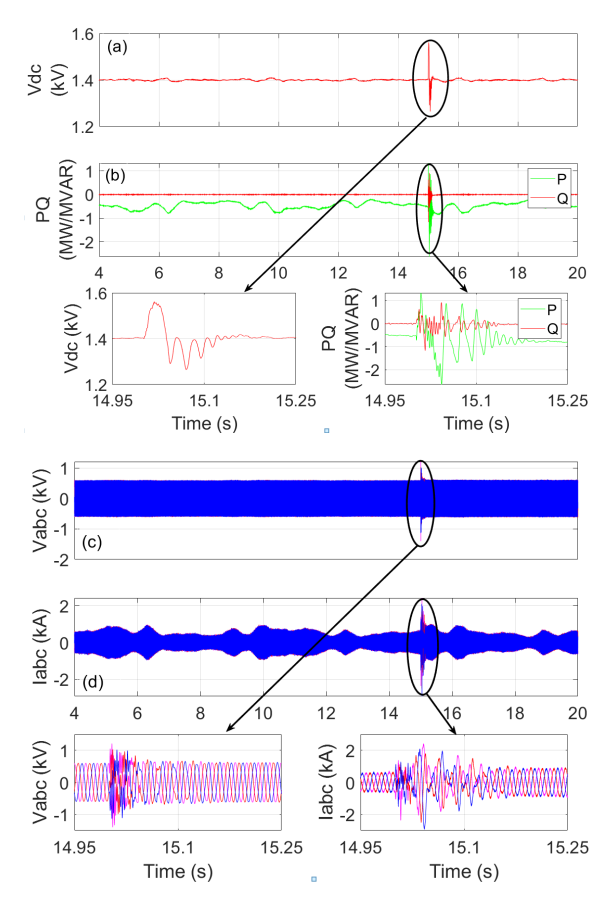


Fig. 11: An abnormal operation of the PMSG WT due to the capacitor bank switching. a) voltage at the dc-link, b) active and reactive power injected to the PCC, c) Three-phase voltages at the PCC, and d) Three-phase currents at the PCC.

common switching on and off of utility capacitor banks [13]. It is pointed out in [13] that the abnormal operation of the wind farms and a lack of a clear industry guideline have confused all involved parties. The wind speed is the same as that of of Fig. 9(a) and 250 WTs are connected online in the wind farm. Similar to [13], a capacitor bank of 50MVar is added at the connection point of the wind farm with the grid to meet the reactive power compensation requirement, and another utility capacitor banks of 500MVar is connected at the substation bus and may switch on and off routinely. Fig. 11 shows the result of this case study. When the substation capacitor banks were switched on at t=15sec, a sharp voltage boost (approximately 1.75 p.u.) appeared at the WT PCC (Fig. 11c), which caused the WT PQ capability region to shrink sharply. This made the GSC of the WTs into an overmodulation operation mode after t=15sec and triggered an abnormal operation event, which would trip the WTs and result in the power generation loss of the wind farm. The result of this case study is consistent with the real-case result reported in [13] and explains the root cause of the abnormal operation of the Type-4 wind farm.

VIII. CONCLUSION

The P-Q capability chart is one of the crucial factors for the design and control of a grid-connected PMSG WT. Proper chart selection ensures the stability and reliability of the overall grid operation. In this paper, an extensive dynamic P-Q capability analysis of a PMSG WT have been performed considering control topology, constraints, and variable grid conditions. The study reveals that the PMSG WT P-Q capability is dynamic and distinct from the standards specified by the power industry. PMSG design parameters, such as, pole pair is an important parameter to specify PMSG P-O capability charts. The study also finds that changes in dc-link voltage and PCC voltage in the real-life situations have a big impact on the P-Q capability chart. PMSG P-Q capability region may shrink due to the PWM modulation technique used and constraints of both power converters. This paper may guide the power community to identify the root cause of many abnormalities associated with the grid-connected PMSG WTs. The proposed study would also help legislators to improve the industry guidelines and introduce new control methods to get over the recent SSO incidents.

IX. ACKNOWLEDGEMENT

This work is supported by National Science Foundation under grant numbers 2141067 and 2137275.

REFERENCES

- N. Nilsson and J. Mercurio, "Synchronous generator capability curve testing and evaluation," *IEEE Trans. Power Del.*, vol. 9, no. 1, pp. 414– 424, Jan 1994.
- [2] Reliability guideline bps-connected inverter-based resource performance. https://www.nerc.com/comm/OC_ReliabilityGuidelines_DL/ Inverter-Based_Resource_Performance_Guideline.pdf. North American Electric Reliability Corporation (NERC) [Online; accessed Sep-2018].
- [3] Inverter-based resource (IBR) workshop. http://ercot.com/content/wcm/ key_documents_lists/176763/ERCOT_IBR_Workshop_April_25_2019. pdf. Electric Reliability Council of Texas (ERCOT).
- [4] L. Soderlund and J. T. Eriksson, "A permanent-magnet generator for wind power applications," *IEEE Trans. Magn.*, vol. 32, no. 4, pp. 2389– 2392, Jul. 1996.
- [5] H. Hojabri, H. Mokhtari, and L. Chang, "Reactive power control of permanent-magnet synchronous wind generator with matrix converter," *IEEE Trans. Power Del.*, vol. 28, no. 2, pp. 575–584, Apr. 2013.
- IEEE Trans. Power Del., vol. 28, no. 2, pp. 575–584, Apr. 2013.
 [6] J. Khazaei, D. H. Nguyen, and A. Asrari, "Consensus-based demand response of PMSG wind turbines with distributed energy storage considering capability curves," *IEEE Trans. Sustain. Energy*, vol. 11, no. 4, pp. 2315–2325, Oct. 2020.
- [7] H. Geng, G. Yang, D. Xu, and B. Wu, "Unified power control for PMSG-based WECS operating under different grid conditions," *IEEE Trans. Energy Convers.*, vol. 26, no. 3, pp. 822–823, Sep. 2011.
- [8] M. J. Dehkordi, S. V. Zadeh, and J. Mohammadi, "Development of a combined control system to improve the performance of a PMSG-based wind energy conversion system under normal and grid fault conditions," *IEEE Trans. Energy Convers.*, vol. 34, no. 3, pp. 1287–1295, Sep. 2019.
- [9] R. H. Ramakrishna, Z. Miao, and L. Fan, "Dynamic performance of type-4 wind with synchronous condenser during weak grids and faults," *IEEE Power Energy Soc. General Meeting*, 2021.
- [10] B. Lu, S. Li, H. S. Das, Y. Gao, J. Wang, and M. Baggu, "Dynamic p-q capability and abnormal operation analysis of a wind turbine with doubly-fed induction generator," *IEEE J. Emerg. Sel. Topics Power Electron.*, vol. 10, no. 4, pp. 4854 4864, Dec 2021.
- [11] N. Miller, J. Sanchez-Gasca, W. Price, and R. Delmerico, "Dynamic modeling of GE 1.5 and 3.6 MW wind turbine-generators for stability simulations," *IEEE Power Energy Soc. General Meeting*, 2003.
- [12] B. Wu, Y. Lang, N. Zargari, and S. Kouro, "Power conversion and control of wind energy systems," *John Wiley & Sons Inc.*, Hoboken, New Jersey, U.S.A. 2011.
- [13] C. Li, "On capacitor switching transient immunity of inverter-based renewable generations," *IEEE Trans. Power Del.*, vol. 30, no. 5, pp. 2339–2345, Oct. 2015.